Rotational vibrational–rotational Raman differential absorption lidar for atmospheric ozone measurements: methodology and experiment

Jens Reichardt, Scott E. Bisson, Susanne Reichardt, Claus Weitkamp, and Bernd Neidhart

A single-laser Raman differential absorption lidar (DIAL) for ozone measurements in clouds is proposed. An injection-locked XeCl excimer laser serves as the radiation source. The ozone molecule number density is calculated from the differential absorption of the anti-Stokes rotational Raman return signals from molecular nitrogen and oxygen as the on-resonance wavelength and the vibrational–rotational Raman backscattering from molecular nitrogen or oxygen as the off-resonance wavelength. Model calculations show that the main advantage of the new rotational vibrational–rotational (RVR) Raman DIAL over conventional Raman DIAL is a 70–85% reduction in the wavelength-dependent effects of cloud-particle scattering on the measured ozone concentration; furthermore the complexity of the apparatus is reduced substantially. We describe a RVR Raman DIAL setup that uses a narrow-band interference-filter polychromator as the lidar receiver. Single-laser ozone measurements in the troposphere and lower stratosphere are presented, and it is shown that on further improvement of the receiver performance, ozone measurements in clouds are attainable with the filter–polychromator approach.

OCIS codes: 010.3640, 280.1910, 290.5860, 010.4950, 290.1090, 290.4210.

1. Introduction

The lidar variant used for ozone measurements in clouds is conventional Raman differential absorption lidar[1,2] (DIAL), with two primary wavelengths transmitted into the atmosphere and ozone calculated from the differential absorption of the corresponding inelastic molecular return signals of molecular nitrogen. As the Raman DIAL error analysis shows, the largest term in the total measurement uncertainty is due to wavelength-dependent multiple scattering and extinction by cloud particles. Its magnitude can be quite substantial,[3,4] hampering the study of cloud-related dynamic and chemical processes that affect ozone.[5,6]

To overcome this problem, a novel technique has been developed that reduces these uncertainties and eliminates the need for a second laser or for generating off-resonance laser radiation by Raman shifting. The approach is based on differential absorption by ozone of the purely rotational Raman return signals from molecular nitrogen and oxygen as the on-resonance wavelength and the vibrational–rotational Raman return from molecular nitrogen or oxygen as the off-resonance wavelength. Because of this combination, rotational vibrational–rotational (RVR) Raman DIAL might be an appropriate term for the new method.

The methodology of the RVR Raman DIAL is developed, and first experimental results are presented. In Section 2 we outline a formalism that we derived for measurements with the RVR Raman DIAL technique. In Section 3 we compare the model calculations of its performance with conventional Raman DIAL for ozone measurements in upper-troposphere cirrus clouds. In Section 4 we provide a detailed description of the first experimental RVR Raman DIAL setup at the Combustion Research Facility,

When this research was performed, J. Reichardt, C. Weitkamp (claus.weitkamp@gkss.de), and B. Neidhart (bernd.neidhart@gkss.de) were with the Institut für Physikalische und Chemische Analytik, GKSS-Forschungszentrum Geesthacht GmbH, Postfach 1160, D-21494 Geesthacht, Germany. J. Reichardt (reichardt@code916.gsfc.nasa.gov) is now with the Joint Center for Earth Systems Technology, University of Maryland Baltimore County, Laboratory for Atmospheres, Code 916, NASA Goddard Space Flight Center, Greenbelt, Maryland 20771. S. E. Bisson (sebisso@sandia.gov) is with Sandia National Laboratories, Livermore, California 94551-0969. S. Reichardt is at 9709 Evening Primrose Drive, Laurel, Maryland 20723.

Received 1 December 1999; revised manuscript received 3 July 2000.

0003-6935/00/336072-08$15.00/0

Sandia National Laboratories, Calif. In Section 5 we present and discuss lidar measurements; in Section 6 we provide a summary.

2. Theory

The RVR Raman DIAL measurement yields the numbers $N(\lambda, z)$ of lidar return photons from distance z at the rotational Raman wavelength λ_R of molecular oxygen and nitrogen and at the vibrational–rotational Raman wavelength λ_{VR} of O_2 or N_2, if light of the primary wavelength λ_L is transmitted. When absorption by particles and trace gases other than ozone is neglected, a condition satisfied for cirrus measurements in the free troposphere,[3] the RVR Raman DIAL ozone molecule number density $n(z)$ in the single-scattering approximation is given by

$$n(z) = RVRN - RVRM - RVRP, \tag{1}$$

where

$$RVRN = \frac{(\mathrm{d}/\mathrm{d}z)\ln[N(\lambda_{VR}, z)/N(\lambda_R, z)]}{C_{O_3}^{abs}(\lambda_R, T) - C_{O_3}^{abs}(\lambda_{VR}, T)},$$

$$RVRM = \frac{\alpha_{mol}^{sca}(\lambda_R, z) - \alpha_{mol}^{sca}(\lambda_{VR}, z)}{C_{O_3}^{abs}(\lambda_R, T) - C_{O_3}^{abs}(\lambda_{VR}, T)},$$

$$RVRP = \frac{\alpha_{par}^{sca}(\lambda_R, z) - \alpha_{par}^{sca}(\lambda_{VR}, z)}{C_{O_3}^{abs}(\lambda_R, T) - C_{O_3}^{abs}(\lambda_{VR}, T)}.$$

Here $C_{O_3}^{abs}(\lambda, T)$ is the ozone absorption cross section at temperature T, and $\alpha_{mol}^{sca}(\lambda, z)$ and $\alpha_{par}^{sca}(\lambda, z)$ are the Rayleigh extinction and the single-scattering particle extinction coefficient, respectively. Similar expressions, *RDN*, *RDM*, and *RDP*, have been derived for conventional Raman DIAL.[4]

Extinction that is due to Rayleigh scattering and hence *RVRM* can be calculated easily from the radiosonde data of weather service stations close to the lidar site. Applying the Raman lidar technique[7] to the Rayleigh-extinction-corrected vibrational–rotational Raman return signal at λ_{VR} yields

$$\frac{\mathrm{d}}{\mathrm{d}z}\ln N(\lambda_{VR}, z) = [\alpha_{par}^{sca}(\lambda_L, z) + \alpha_{par}^{sca}(\lambda_{VR}, z)] + n(z) \times [C_{O_3}^{abs}(\lambda_L, T) + C_{O_3}^{abs}(\lambda_{VR}, T)]. \tag{2}$$

On the assumption that the wavelength dependence of the particle extinction is $\propto \lambda^{\kappa}$, Eqs. (1) and (2) can be solved for the ozone molecule number density $n(z)$ and the particle extinction coefficient $\alpha_{par}^{sca}(\lambda_L, z) \approx \alpha_{par}^{sca}(\lambda_R, z)$. A systematic ozone error is introduced by the term *RVRP* because κ is not well known for the different types of atmospheric particulate scatterers.

In optically dense scattering media or in cirrus clouds, the single-scattering approach is not sufficient and the influence of multiple scattering must be considered. Following the same approach as for the conventional Raman DIAL technique outlined in Ref. 4, we can account for multiple scattering in clouds with particle extinction coefficients $\gtrsim 0.1\ \mathrm{km}^{-1}$ (contribution of scattering by molecules within the cloud negligible) by rewriting *RVRP* as

$$RVRP = \frac{\alpha_{par}^{sca,eff}(\lambda_L, z) + \alpha_{par}^{sca,eff}(\lambda_{VR}, z)}{C_{O_3}^{abs}(\lambda_R, T) - C_{O_3}^{abs}(\lambda_{VR}, T)} \times \Phi[F_R(\lambda_L, z), F_{VR}(\lambda_L, z), \kappa], \tag{3}$$

with the particle correction function

$$\Phi[F_R(\lambda_L, z), F_{VR}(\lambda_L, z), \kappa] = \frac{1 - F_R(\lambda_L, z)}{1 - F_{VR}(\lambda_L, z)} \times \frac{2}{1 + (\lambda_{VR}/\lambda_R)^{\kappa}} - 1. \tag{4}$$

Here $\alpha_{par}^{sca,eff}$ is the measured effective particle extinction, and F_R and F_{VR} are the multiple-scattering parameters[4,8] of the rotational and the vibrational–rotational Raman return signals. Φ depends on the scattering properties of the atmospheric particles.

Because a promising field of application of the RVR Raman DIAL technique is the simultaneous observation of cirrus clouds and ozone concentrations in the free troposphere,[9–12] we chose a RVR Raman DIAL laser wavelength λ_L of approximately 308 nm within the excitation spectrum of XeCl because this is the on-resonance wavelength of most upper-troposphere and stratosphere conventional ozone Raman DIAL's. Note, however, that in contrast to the RVR Raman DIAL the former must emit laser light at a second wavelength, usually between 350 and 355 nm, to generate the off-resonance Raman signal. Whereas differential absorption by ozone is approximately the same for both Raman DIAL and RVR Raman DIAL, the wavelength separation between the on-line and the off-line signals is much smaller in RVR Raman DIAL (Table 1). The new technique is therefore far less sensitive to differential Rayleigh scattering and to wavelength-dependent cloud effects such as multiple scattering and particle extinction. This reasoning is substantiated in Section 3. Note that, if ozone and cloud measurements in the boundary layer rather than in the free troposphere are of primary interest, it could be advantageous to use lidar wavelengths that are shorter than 308 nm. Then single-laser Raman DIAL measurements could also be made by exploitation of the differential absorption by ozone at the vibrational–rotational Raman wavelengths of molecular oxygen and nitrogen [vibrational–rotational vibrational–rotational (VRVR) Raman DIAL]. The theory formulated here applies to the VRVR Raman DIAL as well.

3. Model Calculations

Table 1 lists a summary of the lidar parameters that are assumed for the comparison of O_2 RVR Raman DIAL, N_2 RVR Raman DIAL, and conventional Raman DIAL. First, the case of negligible multiple-scattering effects is considered; in this case the multiple-scattering parameters in *RVRP* [Eq. (3)] and in the corresponding term *RDP* of the Raman DIAL equation[4] are zero. This condition is met

Table 1. Parameters of the Conventional Raman DIAL and the RVR Raman DIAL's[a]

Lidar	On-Resonance Raman Wavelength (nm)	On-Resonance λ_L (nm)	Off-Resonance Raman Wavelength (nm)	Off-Resonance λ_L (nm)	$\Delta\lambda$ (nm)	$\Delta C_{O_3}^{abs}$ (10^{-24} m^2)
O_2 RVR Raman DIAL	307	308	323	308	16	11.7
N_2 RVR Raman DIAL	307	308	332	308	25	12.3
Raman DIAL	332	308	387	355	79	12.4

[a] $\Delta\lambda$, maximum spectral separation of the signals used for the measurements. Differential ozone absorption cross sections ($\Delta C_{O_3}^{abs}$) are calculated from Ref. 13 (T = 226 K). Wavelength values are rounded to full nanometers.

when small particles of relatively low number density dominate atmospheric particulate scattering such as in tropospheric and stratospheric aerosol layers. The relationship between systematic ozone uncertainty, κ uncertainty, and the particle extinction coefficient is shown in Fig. 1. For the calculations we set the ozone molecule number density to 0.7×10^{18} m^{-3}. As expected, owing to the smaller wavelength separation between the on- and off-resonance signals (Table 1), the performance of the RVR Raman DIAL is superior to that of conventional Raman DIAL, and O_2 RVR Raman DIAL performs better than N_2 RVR Raman DIAL. The results are easily extrapolated to other ozone concentrations because it can be shown that for given uncertainties in ozone and κ the acceptable particle extinction coefficient is linear in the molecule number density of the ambient ozone.

Reference 4 provides a detailed discussion of the multiple-scattering effect on ozone measurements with conventional Raman DIAL. To quantify the advantage of the RVR Raman DIAL over conventional Raman DIAL, it is sufficient for one to compare both techniques under some simplifying assumptions:

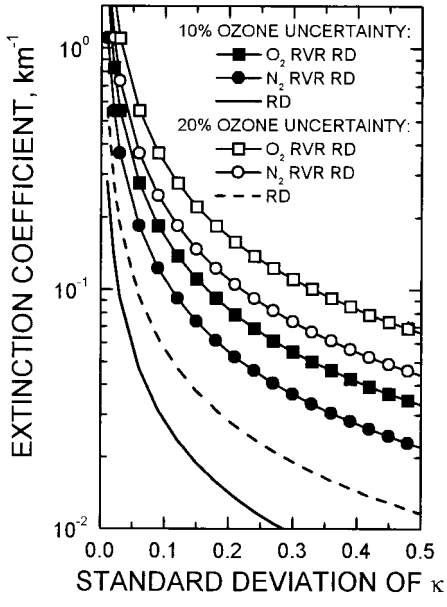

Fig. 1. Relation between the particle extinction coefficient and uncertainty in κ for a given ozone systematic uncertainty: RD, Raman DIAL.

Only the limiting case of optically thick clouds (negligible molecular scattering) is studied, no dependences on lidar system parameters are discussed, and the model cloud considered is homogeneous in particle properties and particle number density throughout its vertical extent. Additionally, the cloud-particle extinction coefficient is supposed to be wavelength independent (κ = 0); particle correction functions calculated with this assumption are denoted Φ_0.

The multiple-scattering model[4,8] that is used for the calculations accounts for the wavelength shift between λ_L and λ_{VR}. The model input parameter, which describes the scattering behavior of the cloud particle ensemble, is the scattering phase function p. For cirrus, the type of cloud under investigation here, p must be determined in the geometrical-optics approximation. At the time this paper was written no crystal phase functions at the RVR Raman DIAL off-resonance wavelengths (323 or 332 nm) were available to the authors. Instead, phase functions of ensembles of ice spheres that are projection-area equivalent to randomly oriented imperfect hexagonal crystals[14] are used for the multiple-scattering computations, because these phase functions can be determined with Mie theory. This approach is justified by the fact that multiple-scattering parameters obtained with phase functions of the two particle classes are almost identical.[8]

Figure 2 shows particle correction functions in cirrus clouds consisting of imperfect hexagonal columns or plates. The RVR Raman DIAL substantially reduces the influence of multiple scattering on ozone measurements. Compared with conventional Raman DIAL, Φ_0 is a factor of ~3.5 and 5.5 smaller for, respectively, N_2 and O_2 RVR Raman DIAL, relatively independently of particle shape and penetration depth. These factors are close to the ratios of the $\Delta\lambda$ value of the conventional Raman DIAL to the corresponding $\Delta\lambda$ values of N_2 and O_2 RVR Raman DIAL (Table 1). From Eq. (3) and from the fact that the differential ozone absorption cross sections of all three lidars are approximately the same, it follows that reductions in Φ_0 translate directly into decreases in the multiple-scattering effect on ozone measurements; e. g., given a cirrus extinction coefficient of 0.1 km^{-1} and a Raman DIAL Φ_0 of -0.04 (Fig. 2), *RDP* becomes -0.65×10^{18} m^{-3} for the conventional Raman DIAL, and *RVRP* is -0.19×10^{18} and $-0.12 \times$

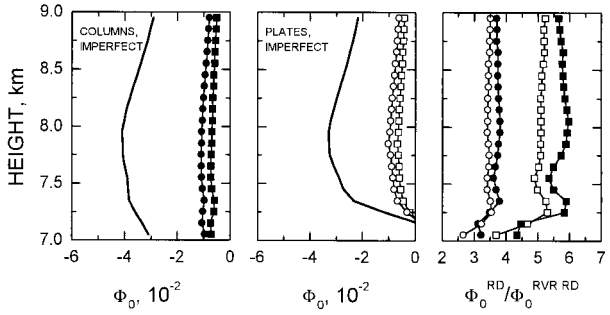

Fig. 2. Particle correction functions Φ_0 of imperfect hexagonal columns (left) and plates (center) for O_2 RVR Raman DIAL (curves with squares), N_2 RVR Raman DIAL (curves with circles) and conventional Raman DIAL (solid curves), and ratios of conventional Raman DIAL Φ_0 to corresponding RVR Raman DIAL Φ_0 (right) in cirrus. Index 0 indicates the presupposed wavelength independence of the particle extinction coefficient. Cirrus-crystal diameters range between 20 and 200 μm. A size distribution from Ref. 15 was used. The receiver field of view is 0.6 mrad.

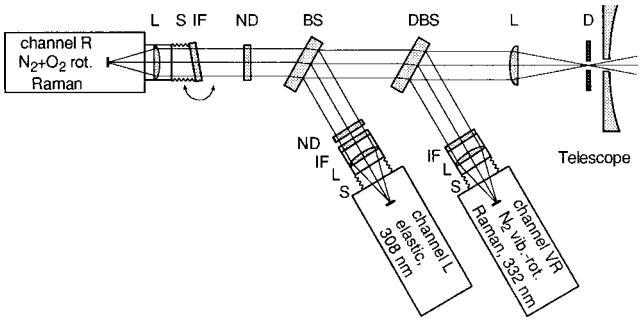

Fig. 3. RVR Raman DIAL receiver: D, diaphragm; L, lens; DBS, dichroic beam splitter; BS, beam splitter; ND, neutral-density filter; IF, interference filter; S, flexible shield. Atmospheric rotational Raman, elastic, and N_2 vibrational–rotational Raman backscattering signals are detected in channels R, L, and VR. The center wavelength of the channel-R interference filter can be tuned by rotating the filter around the vertical axis.

10^{18} m^{-3} for the N_2 and O_2 RVR Raman DIAL, respectively.

4. Experimental Setup

The first experimental RVR Raman DIAL was installed in the trailer of the water-vapor Raman lidar[16] of Sandia National Laboratories, Livermore, Calif. A Lambda Physik LPX 150 T MSC XeCl excimer laser served as the tunable narrow-band radiation source, injection locked at a wavelength of λ_L = 307.94 nm. Optionally a Lambda Physik LPX 220i XeCl excimer laser was used to amplify the output power of typically 12 W to more than 40 W. After beam expansion by a factor of 5 the laser pulses were transmitted into the atmosphere. The spectral purity of the outgoing light was monitored on line. We determined that the laser system can be considered an ideal narrow-band transmitter for the ozone measurements for two reasons. First, during hours of seeded laser operation, we did not observe the buildup of scavenging sidebands or amplified spontaneous emission. Second, tuning the laser wavelength to 307.94 nm (close to the short-wavelength boundary of the broadband excitation spectrum of XeCl) and using the anti-Stokes branch of molecular nitrogen and oxygen rotational Raman scattering as the on-resonance signal for the lidar measurements further reduce considerably the influence of possible unseeded laser pulses or amplified spontaneous emission.

A schematic diagram of the receiving system is shown in Fig. 3. The atmospheric return signal is collected with a 760-mm-diameter Cassegrain telescope (f/4.5) and focused on an adjustable diaphragm serving as the field stop. Apertures of 1–3 mm and corresponding divergences of the collimated light inside the receiver of 6.3–19.0 mrad are usually chosen for the experiments. In this setup, radiation backscattered from N_2 vibrational–rotational Raman scattering is chosen as the off-resonance signal, which is separated from the return signals at shorter wavelengths by a dichroic beam splitter. After the off-resonance signal passes through an interference filter [center wavelength (CWL), 332 nm; FWHM, 2 nm], it is detected in channel VR. The atmospheric signal around 307.94 nm is divided by a beam splitter (92% transmission) for the detection of elastic (channel L; interference filter, 308-nm CWL, 2-nm FWHM) and rotational Raman backscatter light (channel R). The channel-R interference filter is mounted on a precision rotary stage to permit fine tuning of the center wavelength by tilting. Both channels R and L can be protected from the intense short-distance return signals by optional neutral-density filters. The photomultipliers are operated in the photon-counting mode; the data-acquisition electronics is triggered by the stray light of the transmitted pulses. The range bins of the multichannel scalers are set to 75 m; 1000 range bins are stored on a hard disk every 120 s of measurement time. Note that the RVR Raman DIAL is a single-laser ozone lidar. Therefore this system is much less complex than free-troposphere lower-stratosphere conventional DIAL's and Raman DIAL's that all require two radiation sources.

For on-resonance wavelength λ_R, calculations were carried out to optimize the channel-R filter bandwidth and center wavelength for minimum dependence of the return signal on atmospheric temperature and for maximum signal intensity.[17] An important constraint on these considerations is the filter performance at wavelength λ_L because the high suppression of elastically backscattered radiation is crucial for the ozone measurement. It turns out that filters with a center wavelength of 307.4 nm and a bandwidth between 0.3 and 0.5 nm are the best choice. Here temperature effects are well below 0.5% for temperature differences of 50 K, and 60–80% of the intensity of the anti-Stokes branch lies within the bandpass of the filter. This is equivalent to 10–12 times the vibrational–rotational signal intensity of molecular nitrogen.

The channel-R interference filter used for the mea-

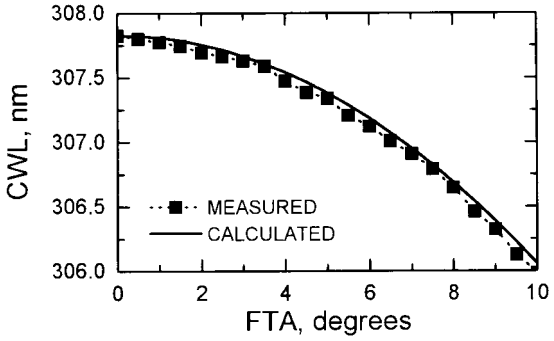

Fig. 4. Dependence of channel-R interference filter center wavelength on the FTA.

surements presented here has a CWL at normal incidence (CWL_0) of 307.81 nm and 0.4-nm FWHM. The measured dependence of the CWL on the angle of incidence and thus on the filter tilt angle (FTA) α is shown in Fig. 4. $CWL(\alpha) = CWL_0\,[1 - (\sin \alpha/n_e)^2]^{1/2}$, which holds for small α and which is used for discussion of the results in Section 5, is plotted as well. Here n_e represents the effective refractive index of the filter ($n_e = 1.62$ according to the manufacturer). With the measured channel-R filter transmission curve, the intensity and the dependence on the atmospheric temperature of the rotational Raman signal impinging on the detector can be calculated as a function of the filter CWL (Fig. 5). Evidently a CWL between 307.33 and 307.39 nm should be chosen for the measurements; this optimum wavelength interval corresponds to a filter tilt angle of ~5° (see Fig. 4). At this angle of incidence the ratio of transmissivity at the filter CWL to transmissivity at the laser wavelength, $\lambda_L = 307.94$ nm, is 830. Mainly because of a poor CWL transmissivity of 5%, the detectable intensity is relatively low. However, 2% of the intensity of atmospheric rotational Raman backscattering is slightly more than the signal strength that can be expected from molecular nitrogen, or oxygen, vibrational–rotational Raman scattering. Therefore, even with this low filter transmissivity, statistical errors of RVR Raman DIAL measurements are smaller than those of measurements with the conventional Raman DIAL, assuming the same lidar parameters. This RVR system advantage will be particularly important when combined with future advances in filter technology.

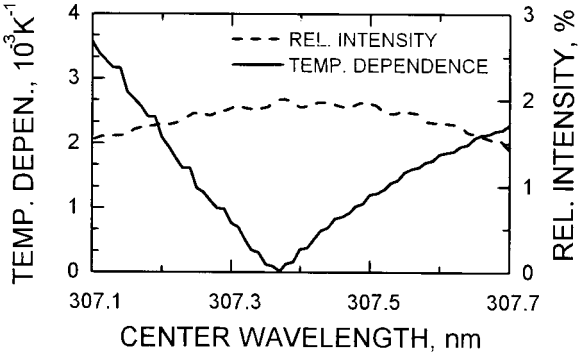

Fig. 5. Intensity and dependence on the atmospheric temperature of the rotational Raman signal impinging on the detector as a function of the channel-R interference filter CWL. The intensity is given relative to the integrated anti-Stokes and Stokes rotational Raman backscattering cross section of N_2 and O_2 with atmospheric mixing ratios. The temperature dependence is obtained from computations carried out for 200- and 250-K atmospheric temperature. For the calculations we used the measured transmission curve of the channel-R filter.

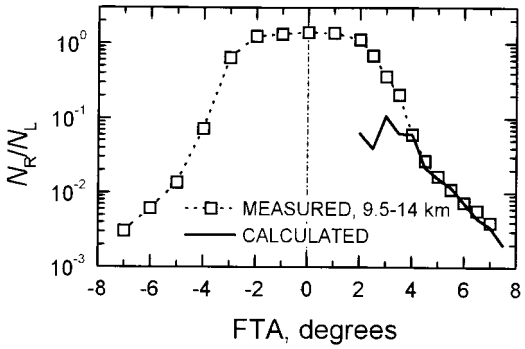

Fig. 6. Ratio of channel-R and channel-L signals as a function of the tilt angle of the channel-R interference filter. Normal incidence corresponds to 0°. The measured values are integrals over the height interval from 9.5 to 14 km. During the measurement no clouds were present.

5. Measurements

In Fig. 6 the ratio of the signals detected in channels R and L are given as a function of the tilt angle of the channel-R interference filter. During this experiment no clouds were present. The field stop diameter and the corresponding receiver field of view (RFOV) were 1.5 mm and 0.3 mrad, respectively.

As expected, the measurement curves are symmetric with respect to normal incidence. The data of the integration height intervals from 5 to 9.5 km and from 14 to 18.5 km (not plotted) are the same within the statistical error; the implication is that even for a narrow RFOV the overlap functions of the receiver channels are identical. The angular dependence of the signal ratios follows theoretical predictions closely if channel transmissivities, the shift of the CWL of the channel-R filter with tilt angle, the contribution of elastic light scattering to the channel-R signal, and the backscattering cross-sectional ratio of Rayleigh and rotational Raman scattering are taken into account. The departure of the calculated curve from the measured data in Fig. 6 is due to an overestimation of the suppression of Rayleigh scattering in channel R at small FTA's (see Fig. 8). The dependence of the signal ratio on intrareceiver light divergence has been studied for fixed FTA's, and for tilt angles <5° a slight influence of the divergence is indeed measured. For larger tilt angles the signal ratio is not affected by the divergence of the return signals.

Figure 7 displays a nighttime measurement of a

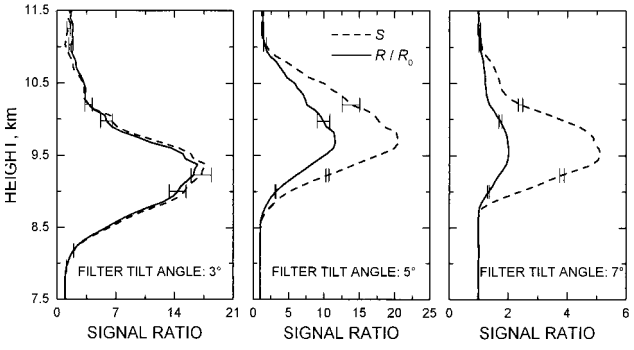

Fig. 7. Time series of R/R_0 (the normalized ratio of the channel-R signal and the channel-VR signal) and of the elastic backscatter ratio S measured during a cirrus event on 17 September 1997. From left to right, the tilt angle of the channel-R interference filter is 3°, 5°, and 7°. The temporal resolution of the profiles is 480 s; the lidar signals are smoothed with a sliding average window length of 600 m. Error bars indicate statistical noise.

cirrus cloud that was taken on 17 September 1997. Obviously, tuning the interference-filter CWL of channel R away from the laser wavelength by increasing the tilt angle reduces drastically the contribution of the elastically backscattered light to the signal of channel R. The suppression, i.e., the quotient of U (the integral of the N_2-rotational-Raman intensity-weighted filter transmission curve over the rotational Raman spectrum) and the transmissivity $T(\lambda_L)$ of the channel-R interference filter, can be computed according to

$$\frac{U}{T(\lambda_L)} = \frac{S(z_{ci})R(z_0) - R(z_{ci})}{[R(z_{ci}) - R(z_0)]V}, \tag{5}$$

where $R(z_0)$ and $R(z_{ci})$ are the ratios of the channel-R signal to the vibrational–rotational Raman signal below and in the cirrus, respectively, $S(z_{ci})$ is the elastic backscatter ratio, and V is constant (Appendix A). In Fig. 8 (left) the experimental results are presented and compared with theoretical $U/T(\lambda_L)$ values derived from the actual, measured transmission curve of the rotational-Raman channel filter. Channel-R

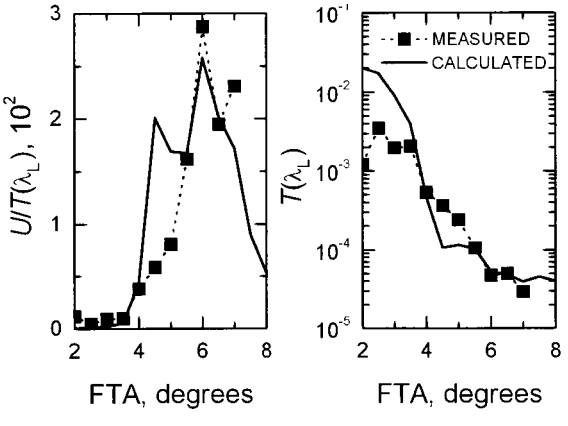

Fig. 8. Suppression $U/T(\lambda_L)$ (left) and transmissivity $T(\lambda_L)$ (right) of the channel-R interference filter as a function of the FTA.

filter transmissivities at primary wavelength λ_L as derived from the atmospheric and the laboratory measurements are also shown (Fig. 8, right). Experimental and calculated data agree well; yet minor differences can be seen. For tilt angles $<3.5°$ the measured suppression $U/T(\lambda_L)$ is higher and the corresponding $T(\lambda_L)$ is lower than the theoretical values. In view of the statistical uncertainties of the cirrus measurement, this may be considered an artifact because S and R/R_0 profiles do not differ significantly for measurements with small FTA's of, e.g., 3° (see Fig. 7). However, the differences in $U/T(\lambda_L)$ and $T(\lambda_L)$ between experiment and theory appear to be systematic since the measured data do not fluctuate around the theoretical curve but are consistently lower and apparently level off toward the small angles. So another possible error source might be channel-R signal nonlinearities during the cirrus measurement that was used for determination of $U/T(\lambda_L)$ and $T(\lambda_L)$. Given the high throughput of the beam splitter (BS, Fig. 3), the return signal that impinges on the detector cathode of channel R is intense for small tilt angles of the channel-R filter. Although neutral-density filters were used to reduce the signal strength, it is quite likely that at the cloud center the signal was still too intense to be detected linearly. In contrast to the case discussed above, $U/T(\lambda_L)$ measured for tilt angles between 4° and 5.5° is smaller and $T(\lambda_L)$ is larger than the theoretical values. The deviations may be explained by the divergence of the return signal. Within the tilt angle interval of steepest change in the transmissivity of elastically backscattered light, photons of wavelength λ_L that hit the interference filter with angles smaller than the mean angle of incidence can contribute significantly to the detected signal. Although the $U/T(\lambda_L)$ data presented are far from being sufficient for measurements of ozone in cirrus, the measurement clearly demonstrates that interference filters can be used to separate rotational Raman from elastically backscattered light in the UV. With two interference filters of slightly improved performance, i.e., higher peak transmission and blocking of primary radiation, in a row, $U/T(\lambda_L)$ values of 10^6 and hence RVR Raman DIAL ozone measurements in clouds should be feasible.

Finally, a single-laser ozone observation with the RVR Raman DIAL is shown in Fig. 9. Clear-sky conditions permitted the choice of a small FTA of 2.8°. Because of problems with the laser the mean output power was only ~5 W during the measurement. Hence the integration time needed for ozone profiling was quite long (3.3 h). Between heights of 3 and 9 km the measured ozone distribution exhibits values around 0.5×10^{18} m^{-3}; in the upper troposphere, smaller ozone molecule number densities are observed. The profile of the ozone mixing ratio, however, is height independent throughout the troposphere with values between 40 and 50 ppbv (parts per billion by volume). The steep onset of the stratospheric ozone layer at 16 km coincides with the tropopause measured with a local radiosonde.

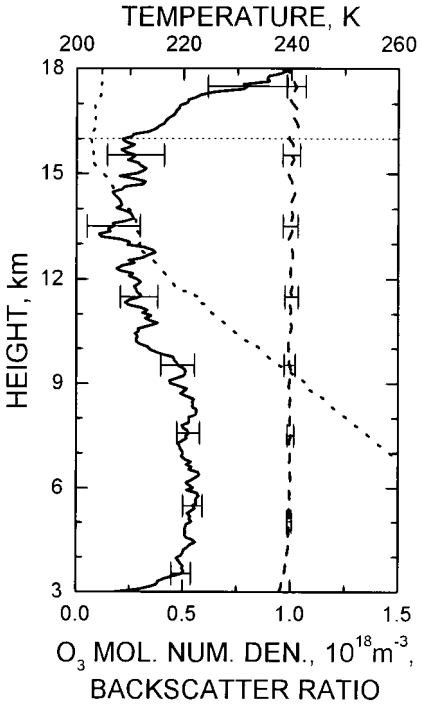

Fig. 9. Ozone molecule number density (solid curve) and backscatter ratio (dashed curve) measured above Livermore, Calif., (37.7 °N, 121.8 °W) on 30 September 1997 between 2154 and 0112 local time. The transmitted laser power was 5 W, and the tilt angle of the channel-R filter was 2.8°. For the ozone calculation the rotational and vibrational–rotational Raman signals are smoothed with sliding average window lengths of 1500 and 2475 m below and above 9.8 km, respectively; values are calculated with a step width of 75 m. Error bars indicate statistical noise. Temperature (dotted curve) and tropopause height (thin dotted line) measured around midnight with a local radiosonde are shown as well.

6. Summary

RVR Raman DIAL for ozone measurements in clouds is a new approach that may well develop into a powerful technique for studies of particle–ozone interactions in the troposphere and lower stratosphere. From model calculations on ozone measurements in upper-troposphere cirrus clouds it is concluded that, independently of the shape and the size of the cirrus particles, RVR Raman DIAL promises to perform in a way far superior to conventional Raman DIAL. Compared with a conventional Raman DIAL, the effects of both wavelength-dependent particle optical extinction and of particle multiple scattering are reduced by ~70% (N_2 RVR Raman DIAL) and ~85% (O_2 RVR Raman DIAL). The first experimental RVR Raman DIAL uses a narrow-band interference-filter polychromator as the lidar receiver. This single-laser ozone lidar setup is much less complex than the free-troposphere and lower-stratosphere conventional DIAL and Raman DIAL systems, which both require two radiation sources.

Ozone profiles were measured with the RVR Raman DIAL in cloud-free atmospheric conditions. Although the suppression of elastically backscattered light in the on-resonance rotational Raman return signal is not yet sufficient for measurements of ozone in cirrus, the measurements show that interference filters can be used to separate the two components of the backscatter spectrum. With two slightly improved interference filters in series, RVR Raman DIAL ozone measurements in clouds should be feasible with the filter–polychromator approach.

Appendix A

The suppression of elastically backscattered radiation by the filter in channel R is defined as the ratio of the integral of the N_2-rotational-Raman intensity-weighted filter transmission curve over the full rotational Raman spectrum (U) to the transmissivity of the filter at the laser wavelength [$T(\lambda_L)$]. $U/T(\lambda_L)$ can be calculated from the measured lidar signals as follows. The number of detected photons in channel R is given by

$$N_R(z) = K' z^{-2}[U\beta^R_{N_2}(z) + T(\lambda_L)S(z)\beta^L_{air}(z)] \times \exp[-\tau(\lambda_L, z)], \quad \text{(A1)}$$

where K' is a height-independent constant; $\beta^R_{N_2}(z)$ and $\beta^L_{air}(z)$ are the volume backscatter coefficients of rotational Raman backscattering from molecular nitrogen and of elastic backscattering from air molecules, respectively; $S(z)$ is the elastic backscatter ratio; and $\tau(\lambda_L, z)$ is the optical depth of the atmosphere (full overlap between the lidar beam and the RFOV assumed). Introducing

$$V = c_{N_2}(dC^{b,R}_{N_2}/d\Omega)/(dC^{b,L}_{air}/d\Omega),$$

where c_{N_2} is the atmospheric N_2 mixing ratio and $dC^{b,R}_{N_2}/d\Omega$ and $dC^{b,L}_{air}/d\Omega$ are the cross sections of the backscattering processes, we obtain

$$N_R(z) = K' z^{-2}[UV + T(\lambda_L)S(z)] \times \beta^L_{air}(z)\exp[-\tau(\lambda_L, z)]. \quad \text{(A2)}$$

$R(z)$, the ratio of $N_R(z)$ to the vibrational–rotational Raman signal

$$N_{VR}(z) = K'' z^{-2}\beta^L_{air}(z)\exp[-\tau(\lambda_L, \lambda_{VR}, z)],$$

where K'' is a constant, can then be written as

$$R(z) = K[UV + T(\lambda_L)S(z)] \times \exp-[\tau(\lambda_L, z) - \tau(\lambda_L, \lambda_{VR}, z)], \quad \text{(A3)}$$

where $K = K'/K''$. Let z_{ci} and z_0 be heights within and slightly below the cirrus cloud. Then we can derive the equation

$$\frac{R(z_{ci})}{R(z_0)} = \frac{UV + T(\lambda_L)S(z_{ci})}{UV + T(\lambda_L)}. \quad \text{(A4)}$$

Here the differential transmission between z_{ci} and z_0 has been neglected. From Eq. (A4) we determine that

$$\frac{U}{T(\lambda_L)} = \frac{S(z_{ci})R(z_0) - R(z_{ci})}{[R(z_{ci}) - R(z_0)]V}. \quad \text{(A5)}$$

We gratefully acknowledge the assistance of Phil Paul, Combustion Research Facility, Sandia National Laboratories, with the alignment of the excimer laser. We also thank Rudolf Baumgart of the Institut für Physikalische und Chemische Analytik at GKSS-Forschungszentrum Geesthacht for the spectral measurements of the rotational-Raman-channel interference filter.

References

1. T. J. McGee, M. Gross, R. Ferrare, W. Heaps, and U. Singh, "Raman DIAL measurements of stratospheric ozone in the presence of volcanic aerosols," Geophys. Res. Lett. **20,** 955–958 (1993).
2. J. Reichardt, U. Wandinger, M. Serwazi, and C. Weitkamp, "Combined Raman lidar for aerosol, ozone, and moisture measurements," Opt. Eng. **35,** 1457–1465 (1996).
3. J. Reichardt, "Optische Fernmessung von Ozon in Zirruswolken," Ph.D. dissertation, Rep. GKSS 98/E/11 (1998) (Universität Hamburg, Hamburg, Germany, 1997).
4. J. Reichardt, "Error analysis of Raman differential absorption lidar ozone measurements in ice clouds," Appl. Opt. **39,** 6058–6071 (2000).
5. R. R. Dickerson, G. J. Huffman, W. T. Luke, L. J. Nunnermacker, K. E. Pickering, A. C. D. Leslie, C. G. Lindsey, W. G. N. Slinn, T. J. Kelly, P. H. Daum, A. C. Delany, J. P. Greenberg, P. R. Zimmerman, J. F. Boatman, J. D. Ray, and D. H. Stedman, "Thunderstorms: an important mechanism in the transport of air pollutants," Science **235,** 460–465 (1987).
6. J. Lelieveld and P. J. Crutzen, "Influences of cloud photochemical processes on tropospheric ozone," Nature (London) **343,** 227–233 (1990).
7. A. Ansmann, M. Riebesell, and C. Weitkamp, "Measurement of atmospheric aerosol extinction profiles with a Raman lidar," Opt. Lett. **15,** 746–748 (1990).
8. J. Reichardt, M. Hess, and A. Macke, "Lidar inelastic multiple-scattering parameters of cirrus particle ensembles determined with geometrical-optics crystal phase functions," Appl. Opt. **39,** 1895–1910 (2000).
9. K. E. Pickering, A. M. Thompson, J. R. Scala, W.-K. Tao, R. R. Dickerson, and J. Simpson, "Free troposphere ozone production following entrainment of urban plumes into deep convection," J. Geophys. Res. **97,** 17,985–18,000 (1992).
10. E. V. Browell, M. A. Fenn, C. F. Butler, W. B. Grant, J. T. Merrill, R. E. Newell, J. D. Bradshaw, S. T. Sandholm, B. E. Anderson, A. R. Bandy, A. S. Bachmeier, D. R. Blake, D. D. Davis, G. L. Gregory, B. G. Heikes, Y. Kondo, S. C. Liu, F. S. Rowland, G. W. Sachse, H. B. Singh, R. W. Talbot, and D. C. Thornton, "Large-scale air mass characteristics observed over Western Pacific during the summertime," J. Geophys. Res. **101,** 1691–1712 (1996).
11. J. Reichardt, A. Ansmann, M. Serwazi, C. Weitkamp, and W. Michaelis, "Unexpectedly low ozone concentration in midlatitude tropospheric ice clouds: a case study," Geophys. Res. Lett. **23,** 1929–1932 (1996).
12. K. Sassen, G. G. Mace, J. Hallett, and M. R. Poellet, "Corona-producing ice clouds: a case study of a cold mid-latitude cirrus layer," Appl. Opt. **37,** 1477–1485 (1998).
13. L. T. Molina and M. J. Molina, "Absolute absorption cross sections of ozone in the 185- to 350-nm wavelength range," J. Geophys. Res. **91,** 14,501–14,508 (1986).
14. M. Hess, R. B. A. Koelemeijer, and P. Stammes, "Scattering matrices of imperfect hexagonal ice crystals," J. Quant. Spectrosc. Radiat. Transfer **60,** 301–308 (1998).
15. A. J. Heymsfield and C. M. R. Platt, "A parameterization of the particle size spectrum of ice clouds in terms of the ambient temperature and the ice water content," J. Atmos. Sci. **41,** 846–855 (1984).
16. S. E. Bisson, J. E. M. Goldsmith, and M. G. Mitchell, "Narrowband, narrow-field-of-view Raman lidar with combined day and night capability for tropospheric water-vapor profile measurements," Appl. Opt. **38,** 1841–1849 (1999).
17. J. Reichardt, C. Weitkamp, and S. Krumbholz, "Rotational vibrational–rotational (RVR) Raman DIAL: a novel lidar technique for atmospheric ozone measurements," in *Proceedings of the 13th ESA Symposium on European Rocket and Balloon Programmes and Related Research*, ESA SP-397 (European Space Agency, Noordwijk, The Netherlands, 1997), pp. 237–241.